Data Paper

Experiments in a Large Boundary Layer Wind Tunnel: Propagation of Noise through the Turbulent Boundary Layer

Tianshu Zhang[1]; Mariel A. Ojeda-Tuz, S.M.ASCE[2]; Kurtis R. Gurley, A.M.ASCE[3]; and Steven A. E. Miller[4]

Abstract: A series of acoustic propagation experiments was conducted in the University of Florida Boundary Layer Wind Tunnel (UFBLWT) to investigate tornadic infrasound propagation in the turbulent atmosphere. A synthetic acoustic wave was generated within a boundary layer wind field using a speaker, and distorted by the surrounding turbulent atmosphere as it propagated along the UFBLWT fetch where it was measured by an acoustic microphone 22 m downwind of the speaker. The wind tunnel operating speed and the configuration of the mechanical turbulence generating roughness elements were varied between experiments to alter the turbulence characteristics and thus the distortion of the acoustic wave. The wind field turbulence data were obtained by three Cobra probes mounted on an actuated and automated gantry. The turbulence-induced distortion of the acoustic wave was captured by analyzing the signal at its source and as-measured downwind. Data were characterized, organized, and curated into four stages. **DOI: 10.1061/(ASCE)ST.1943-541X.0003275.**
© 2022 American Society of Civil Engineers.

Downloaded from ascelibrary.org by Tianshu Zhang on 02/17/22. Copyright ASCE. For personal use only; all rights reserved.

Introduction

Tornadoes are responsible for the devastation of lives, buildings, and infrastructure (Brooks and Doswell 2001). Tornadoes create low-frequency acoustic waves (Frazier et al. 2014) below the threshold of human hearing, called infrasound (Evers and Haak 2010). These acoustic waves travel long distances through the turbulent atmosphere. Although the waves experience very little atmospheric absorption (Bowman and Bedard 1971; Le Pichon et al. 2010), they are altered by atmospheric turbulence. Early warning systems can be improved via triangulation of the source through distributed measurement of the tornado infrasound (Talmadge and Waxler 2016). Acoustic observations of tornadoes (Elbing et al. 2018; Bedard 2005) yield insight into the statistics of the infrasound noise. The peak frequency of the infrasound from a tornado is in the range 5–10 Hz and can be detected over 100 mi from its source (Bedard et al. 2004). To create accurate early warning systems, the influence of atmospheric turbulence on the distortion of infrasound characteristics must be accounted for within the interpretation of measurements and predictive modeling (Talmadge and Waxler 2016; Schimmel and Hübl 2015; Pepyne et al. 2011). A complicating factor is that the nature of the atmospheric turbulence distorting the infrasound changes as a function of both storm conditions and the terrain over which it translates.

The University of Florida (UF) is developing a fast prediction model for infrasound propagation through turbulence for the purposes of predicting tornado formation, tracking tornadoes, and increasing safety via improved early warning. A series of boundary layer wind tunnel experiments was conducted at the University of Florida Boundary Layer Wind Tunnel (UFBLWT) to characterize the distortion of acoustic waves via propagation through atmospheric turbulence. The resultant data set is presented in four stages described in the next section. The experimental procedures and facilities are introduced in the following section. A detailed description of the four-stage experimental campaign then is presented. Example measurements and the data organization then are presented. The last section discusses the limitations and potential applications of the data.

Experimental Procedure and Facilities

Experimental Procedure

The experimental campaign consisted of four measurement stages: (1) the design of the synthetic acoustic wave at its source, (2) the characterization of the background noise associated with turbulence in the UFBLWT at the same location as the acoustic wave measurement, (3) the acoustic wave propagation measurement within turbulence, and (4) turbulence profiles through the depth of the UFBLWT to capture the longitudinal evolution of the boundary layer.

Fig. 1 illustrates the configuration of UFBLWT. The flow is driven by the fan bank, then conditioned by the honeycomb and Irwin spires. Flow then passes the cross-section inlet, after which the boundary layer flow is developed over the fetch of the terraformer section before arriving at the test section.

The positions of the instruments and tunnel coordinates are shown in Fig. 2 for the third and fourth stages of the experiment.

[1]Graduate Research Assistant, Dept. of Mechanical and Aerospace Engineering, Univ. of Florida, Gainesville, FL 32611 (corresponding author). ORCID: https://orcid.org/0000-0002-9556-1139. Email: zhang.tianshu@ufl.edu

[2]Graduate Research Assistant, Engineering School of Sustainable Infrastructure and Environment, Univ. of Florida, Gainesville, FL 32611. ORCID: https://orcid.org/0000-0003-1844-8703. Email: ojedatuzm@ufl.edu

[3]Professor and Engineering School of Sustainable Infrastructure and Environment Associate Director, Engineering School of Sustainable Infrastructure and Environment, Univ. of Florida, Gainesville, FL 32611. Email: kgurl@ce.ufl.edu

[4]Assistant Professor, Dept. of Mechanical and Aerospace Engineering, Univ. of Florida, Gainesville, FL 32611. Email: saem@ufl.edu; saemiller@gmail.com

Note. This manuscript was submitted on June 10, 2021; approved on October 21, 2021; published online on February 17, 2022. Discussion period open until July 17, 2022; separate discussions must be submitted for individual papers. This paper is part of the ***Journal of Structural Engineering***, © ASCE, ISSN 0733-9445.

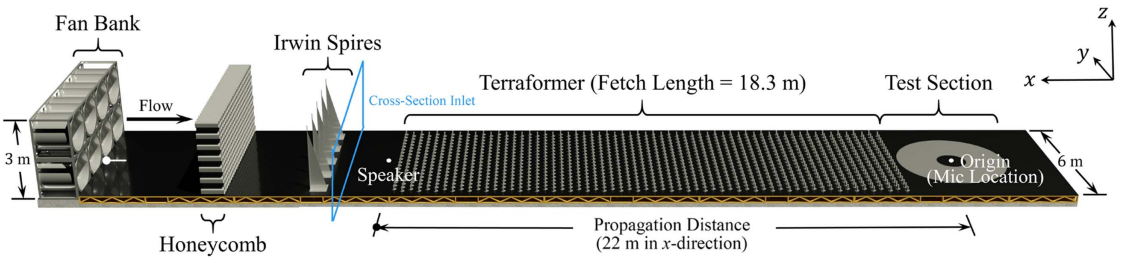

Fig. 1. Microphone and speaker locations along with the UFBLWT configuration.

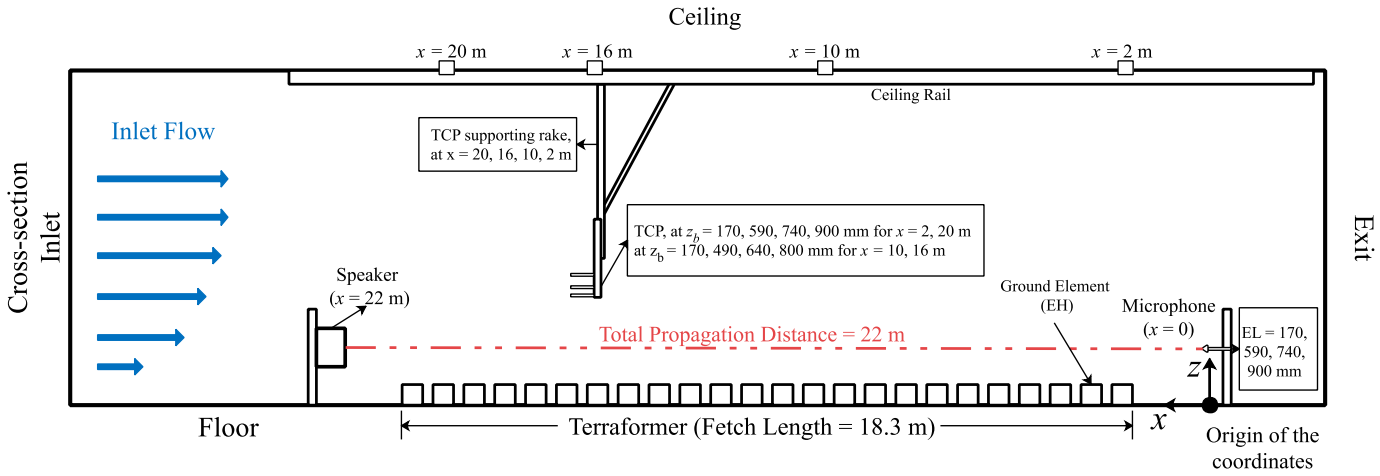

Fig. 2. Coordinates and configuration of the Stage 3 and 4 experiments.

The origin of the coordinate system was located at the center of the test section. The x-direction was defined as upstream from this location, and z represented the vertical direction. In Stage 3, the microphone was located at $x = 0$, and the speaker was placed at $x = 22$ m, near the inlet (Fig. 2). Thus the total propagation distance was fixed at 22 m. For the acoustic test, the elevation height EL was used to represent the distance between the acoustic system and the floor. The turbulent measurements in Stage 4 were conducted by a three-Cobra-probe (TCP) system, which was mounted on a supporting gantry that translated in three dimensions; EH was the pitch height of the ground element, and z_b was the z-location of the bottom probe in TCP system. More details are discussed in the next section.

Stages of Experimental Campaign

For Stage 1, the acoustic wave was designed in MATLAB version 2016b as a single-cycle pulse, and was imparted by a commercial speaker. The speaker introduced an initial distortion (a deviation from its on-paper design) upon the acoustic wave due to the speaker's impulse response. We measured the speaker output in an anechoic chamber to capture the nature of the speaker-produced acoustic wave before it was distorted via propagation through atmospheric turbulence (Stage 3). The microphone and speaker used for Stage 1 were the same devices used in Stages 3 in the UFBLWT.

For Stage 2, the UFBLWT was characterized acoustically by conducting the entire test matrix (multiple wind speeds and turbulent conditions, described subsequently) without the acoustic wave imparted to the flow. The microphone was placed at $x = 0$ at a fixed height, which measured the background noise of the turbulent flow. This allowed for a statistical evaluation of the natural or ambient turbulent noise that had to be separated from the distorted acoustic wave signal in the next stage.

In Stage 3 the acoustic wave was imparted to the flow via the speaker placed upwind of the microphone and roughness element fetch (Fig. 2). The working conditions of the wind tunnel were kept the same as in Stage 2. The acoustic wave was generated at multiple times for each flow condition. Stage 3 and Stage 2 were analyzed to extract the acoustic wave from the background noise, and then its distortion was characterized via comparison with the Stage 1 output for each of the conditions in the test matrix.

Stage 4 was designed to quantify the vertical wind field turbulence profile with high temporal and spatial resolution in order to facilitate the modeling of turbulent scattering effects on acoustic propagation. The TCP was capable of translating in three dimensions, providing vertical turbulence profiles measured at a series of locations through the depth of the UFBLWT along the center line (Fig. 2). By interpolating these profiles in the x-direction, the turbulent statistics were obtained along the ray paths with multiple elevation heights.

Experimental Facilities

UF Mechanical and Aerospace Engineering Anechoic Chamber

Stage 1 experiments were conducted in the anechoic chamber in the UF Mechanical and Aerospace Engineering Building A. The chamber was designed for open-jet aeroacoustic experiments (Mathew et al. 2005b). Anechoic treatments (Brouwer 1997) are applied

Downloaded from ascelibrary.org by Tianshu Zhang on 02/17/22. Copyright ASCE. For personal use only; all rights reserved.

to all the sidewalls, the floor, and the ceiling to minimize acoustic reflection in the chamber. The interior dimensions of the chamber are 5.5 m long by 5 m wide by 2.3 m high, which provided suitable space to measure the speaker's output of the acoustic wave. Fiberglass wedges enclosed by steel meshes provided a cut-off frequency of approximately 100 Hz, which was adequate for the frequency of the acoustic wave, which started at 800 Hz. More details of this chamber were given by Mathew et al. (2005a). The same microphone and speaker were used in the chamber and the UFBLWT acoustic experiments in Stage 3.

University of Florida Turbulent Boundary Layer Wind Tunnel

Stages 2, 3, and 4 were conducted in the UFBLWT at the Powell Family Structures and Materials Laboratory on UF's east campus. The UFBLWT (Fig. 1) is a low-speed wind tunnel with a 6 m wide by 3 m high cross section and over 20 m of fetch between the fans and the test section. Fig. 3 shows the fan bank that drives the flow. Eight 1.5-m Aerovent vane axial fans with adjustable pitch blades can generate up to 16-m/s tunnel velocities. The tunnel has an adjustable ceiling pitch to regain static pressure lost from friction. The UFBLWT offers a unique automated terrain roughness element system (terraformer) which can reconfigure each of 1,116 individual roughness elements within 90 s to achieve desired approach flow conditions (Catarelli et al. 2020b). Many diverse terrain configurations and associated turbulent flows can be investigated rapidly.

Validation studies of the wind field and its relationship to the roughness element configuration have been published recently. These include floor to freestream mean and turbulence profiles for 33 homogeneous terrain configurations (Fernández-Cabán and Masters 2018; Catarelli et al. 2020a), and measured longitudinal velocity spectra (Fernández-Cabán et al. 2018; Fernández-Cabán and Masters 2018, 2020).

The UFBLWT does not have anechoic treatment (Brouwer 1997) and would not be considered as a tunnel that typically is useful for acoustic tests. Wind tunnels created for acoustic testing often have open or partially open test sections (Remillieux et al. 2008; Mathew et al. 2005b), anechoic treatment (Holloway et al. 2002), and special baffles to dampen the acoustic waves from the compressor or electric motor system (Baals 1981; Duell et al. 2013). The present facility was designed primarily to create repeatable and finely tuned atmospheric turbulent boundary layers with varying roughness and scale. The roughness elements scatter noise, which propagates throughout the tunnel (Sovardi et al. 2016). However, this scattered noise lags the incident wave. Furthermore, the walls of the UFBLWT have very little to no acoustic absorption properties, and therefore we treated them as hard walls that approximate perfectly reflected acoustic waves (Pridmore-Brown 1958).

For Stage 2 testing, we placed a bullet-nose microphone [D. C. McCormick, and W. P. Patrick, "Multistage turbulence shield for microphones," US Patent No. 5,808,243 (1998)] at a fixed height in the test section (Fig. 4), and conducted a series of experiments, each of which differed in terms of roughness element height and/or mean wind speed, and thus in turbulence characteristics.

The microphone measured a time history of the turbulence-induced fluctuating pressure during each of these experiments. For Stage 3, this setup was amended by the addition of the speaker (Fig. 5) downwind of the fans and just upwind of the roughness

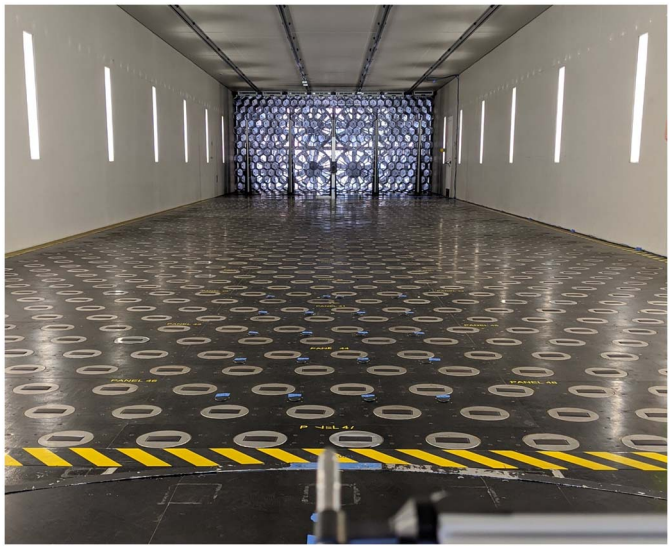

Fig. 3. University of Florida Boundary Layer Wind Tunnel from the test section looking upstream.

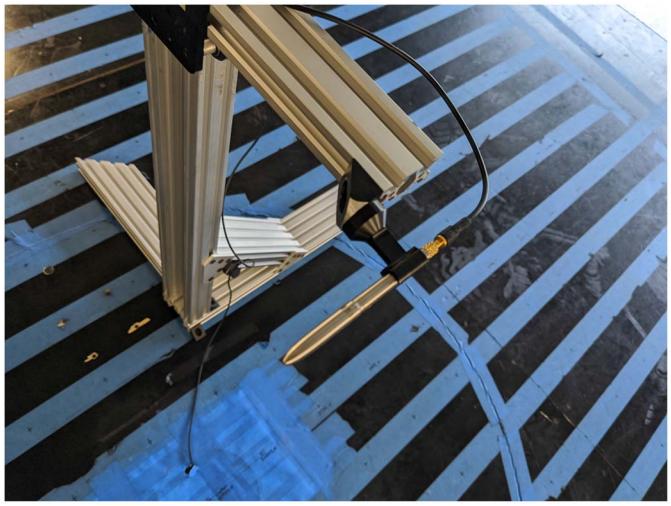

Fig. 4. G.R.A.S. 46BE 1/4-in. CCP free-field standard microphone at $EL = 590$ mm with the supporting system.

Fig. 5. Speaker at $EL = 590$ mm with the supporting system.

Downloaded from ascelibrary.org by Tianshu Zhang on 02/17/22. Copyright ASCE. For personal use only; all rights reserved.

elements, providing 22-m distance between speaker and microphone (Fig. 2).

The same roughness element heights and wind speed combinations from Stage 2 were repeated while the acoustic wave was played repeatedly by the speaker, and the microphone recorded the combined wind tunnel turbulence and distorted acoustic wave. For Stage 4, both the microphone and speaker were removed, and three vertically aligned Cobra probes mounted to an automated gantry (TCP) were moved along the center line of the tunnel to characterize the boundary layer at four locations along the UFBLWT center line (Fig. 2). The Stage 4 test matrix was not as granular with respect to element height configurations as the Stage 2 and 3 test matrices due to time restrictions.

Stages of Experimental Campaign

Stage 1: Acoustic Signal Design and Anechoic Test

Because the UFBLWT is not an anechoic facility, a specific acoustic wave was designed so that it could be isolated relative to the background noise in the tunnel relative to the turbulence. In addition, the reflection from the acoustic wave could be isolated relative to the incident wave using linear theory. The incident and reflected waves were ensemble averaged, and then the background noise from the tunnel was isolated. The acoustic wave was a series of single-cycle sine waves described by two functions. The first was a sine wave S_s as a function of time t (s)

$$S_s(t) = \begin{cases} \sin(2\pi f_1 t) & 0 \le t < 36 \\ \sin(2\pi f_2 t) & 36 \le t < 72 \\ \sin(2\pi f_3 t) & 72 \le t < 108 \\ \sin(2\pi f_4 t) & 108 \le t < 144 \end{cases} \tag{1}$$

where $f_1 = 800$ Hz; $f_2 = 1250$ Hz; $f_3 = 1600$ Hz; and $f_4 = 2000$ Hz. These frequencies were selected to avoid the wind tunnel's characteristic frequencies (discussed in the next section) and to simulate the infrasound via the scaling factors based on the propagation distance through the atmosphere. Typical long-range infrasound propagation distances are on the order of 100 km. The tunnel propagation length was 22 m (the total propagation distance in UFBLWT tests), which resulted in a scaling factor of 4,545.5. Thus, the four frequencies in the UFBLWT propagation experiments were representative of scaled frequencies within the broadband spectrum of tornadic infrasound in atmosphere. To obtain the pulsating single cycles instead of the tonal sounds, a window W was constructed as

$$W(t) = \begin{cases} \sum_{N=1}^{36}\left(H(t-N) - H\left(t-N-\frac{1}{800}\right)\right) & t < 36 \\ \sum_{N=1}^{36}\left(H(t-N-36) - H\left(t-N-36-\frac{1}{1250}\right)\right) & 36 \le t < 72 \\ \sum_{N=1}^{36}\left(H(t-N-72) - H\left(t-N-72-\frac{1}{1600}\right)\right) & 72 \le t < 108 \\ \sum_{N=1}^{36}\left(H(t-N-108) - H\left(t-N-108-\frac{1}{2000}\right)\right) & 108 \le t < 144 \end{cases} \tag{2}$$

where $H(x)$ is the Heaviside function; and N = number of pulses for each frequency. By multiplying the window function W by the S_s signal, the test signal S_t is obtained

$$S_t(t) = W(t)S_s(t) \tag{3}$$

Fig. 6 shows the structure of S_t as 36 repeated cycles for each of the four frequencies. The 36 single cycles of the 800 Hz portion were in period 3–39 s, period 39–5 s was the 1,250 Hz portion, period 75–111 s was the 1,600 Hz portion, and period 111–147 s was the 2,000 Hz portion. Each single cycle is followed by a zero-padding period to assemble a one-second pulse. At the end of the signal, four reminder tones indicated that the operator should stop recording.

This single-cycle test signal was designed to remove acoustic reflections by producing a phase difference between the direct wave and reflected waves. Because the reflected wave traveled a longer distance than the direct wave, the arrival time of the reflected wave was delayed with respect to the direct wave. Because the additional propagation distance of the reflected wave was longer than the wavelength of the test signal, the phase difference guaranteed a

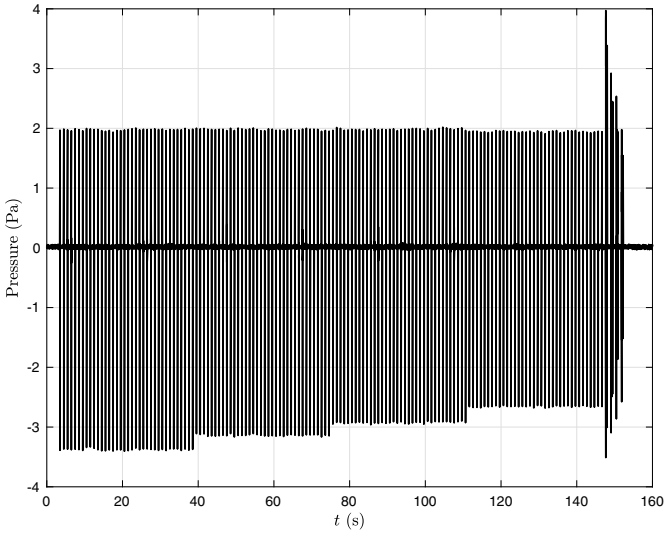

Fig. 6. Raw anechoic chamber source signal recording 2 m from the speaker.

Downloaded from ascelibrary.org by Tianshu Zhang on 02/17/22. Copyright ASCE. For personal use only; all rights reserved.

Downloaded from ascelibrary.org by Tianshu Zhang on 02/17/22. Copyright ASCE. For personal use only; all rights reserved.

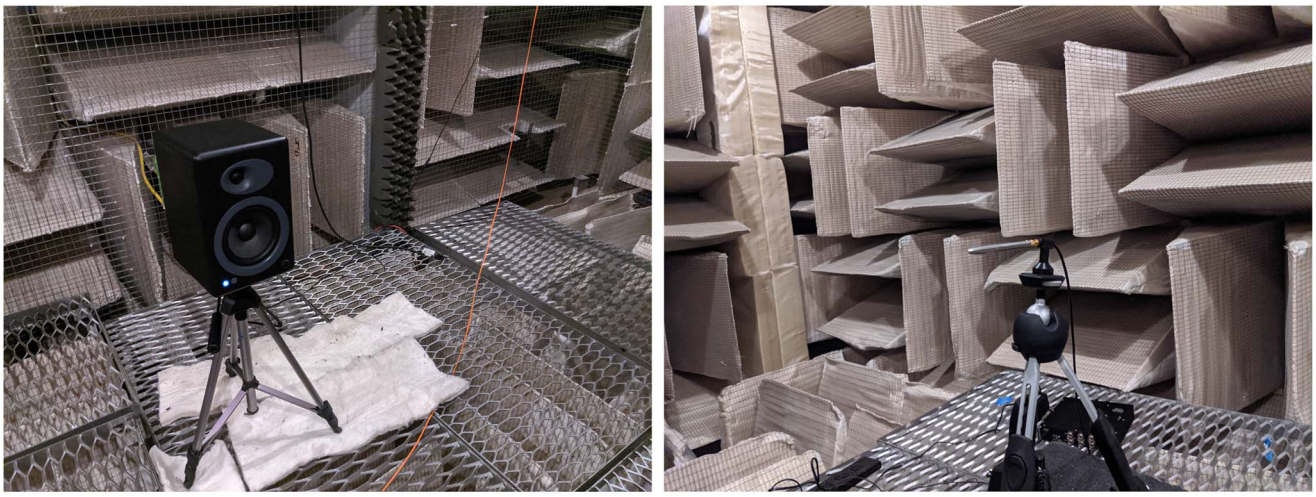

Fig. 7. Acoustic system in anechoic chamber with the propagation distance of 2 m: (a) speaker; and (b) microphone.

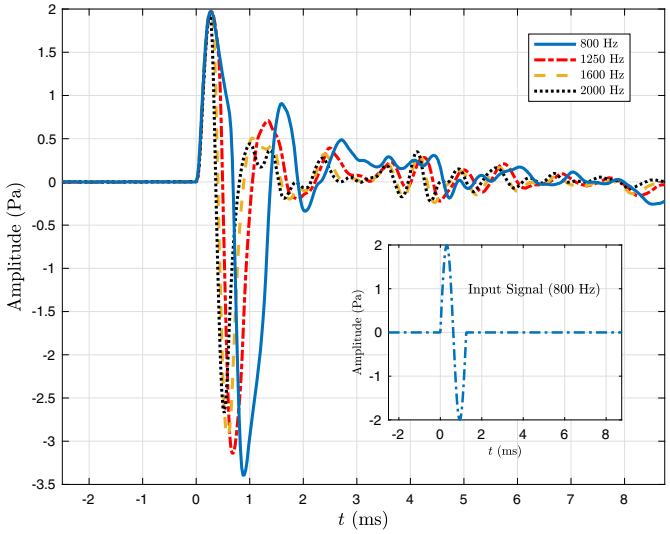

Fig. 8. Output single cycle signals 2 m from speaker.

separation between the direct wave and reflected waves. By taking the ensemble average of the 36 repeated single cycles for each frequency, the broadband turbulent noise was removed efficiently.

The acoustic wave was coded with a MATLAB script and played through a commercial speaker. The Stage 1 speaker test was conducted in the anechoic chamber to characterize precisely the acoustic wave output from the speaker. Fig. 7 shows the speaker and microphone systems in the anechoic chamber test. During the test, the speaker and the microphone were calibrated at the same height to establish a straight-line ray path. The microphone was located 2 and 3 m from the center of the speaker's diaphragm for two separate tests.

Fig. 8 shows the 36-ensemble average of the measured acoustic wave from the anechoic chamber speaker test. The MATLAB-generated input signal of 800 Hz is shown as the dashed line in the figure inset. The 800, 1,250, 1,600, and 2,000-Hz pulses were recorded 2 m from the speaker.

For the first crests of all frequencies, the amplitudes of the troughs were −3.393, −3.136, −2.857, and −2.657 Pa for the 800, 1,250, 1,600, and 2,000 Hz signals, respectively. By comparing with the input signal, the amplifications of the troughs were caused by the impulse response (Everest 2001). This amplitude-strengthening phenomenon also was observed in a previous pulse signal study (Aoshima 1981). The 800-Hz pulse had the most intense impulse response because its trough had the highest magnitude, 3.393 Pa. Because of the impulse response, the speaker's diaphragm kept oscillating after the single-cycle pulse, which differed from the input signal in the figure inset. It took about 20 ms to rest for the 800-Hz signal, whereas the rest time for the 1,600-Hz signal was about 13 ms. To eliminate the impulse responses' interaction, a zero-padding region was placed between the single cycles. The distortion caused by the speaker changed the 800-Hz acoustic waveform significantly from its designed sine-wave like wave form (Fig. 8). Because our speaker was a two-way speaker, the woofer was the major generator of the low-frequency signal relative to the tweeter (Mäkivirta et al. 2018). When the impulse entered the speaker, the phase delay between the woofer and tweeter caused distortion of the 800 Hz signal. Therefore, in the rest of the paper and the postprocessed data, the 800-Hz acoustic wave was removed and is not presented with the experimental results.

Stage 2: UFBLWT Background Noise Characterization

To understand the acoustic character of the wind tunnel, the background turbulence noise within the UFBLWT was characterized using the microphone previoiusly described. To identify the working condition of the wind tunnel, the estimated wind speed WS (based on wind tunnel fan speed estimation) and a pitot tube (Dwyer, Series 600, Michigan City, Indiana)-measured reference wind speed U_{ref} at $x = 1.48$ m and $z = 2.5$ m (near the exit in Fig. 2) were employed for the tests. The spectra of the wind tunnel's background noise are shown in Fig. 9 with $EH = 0$ at U_{ref} corresponding to 0, 3.47 6.85, and 10.62 m/s, respectively.

We observed broadband sound pressure level (SPL) increases from low wind speed to high wind speed, which primarily were introduced by the turbulence within the tunnel. The peak frequencies at 3, 6, and 9 kHz were captured as the characteristic wind

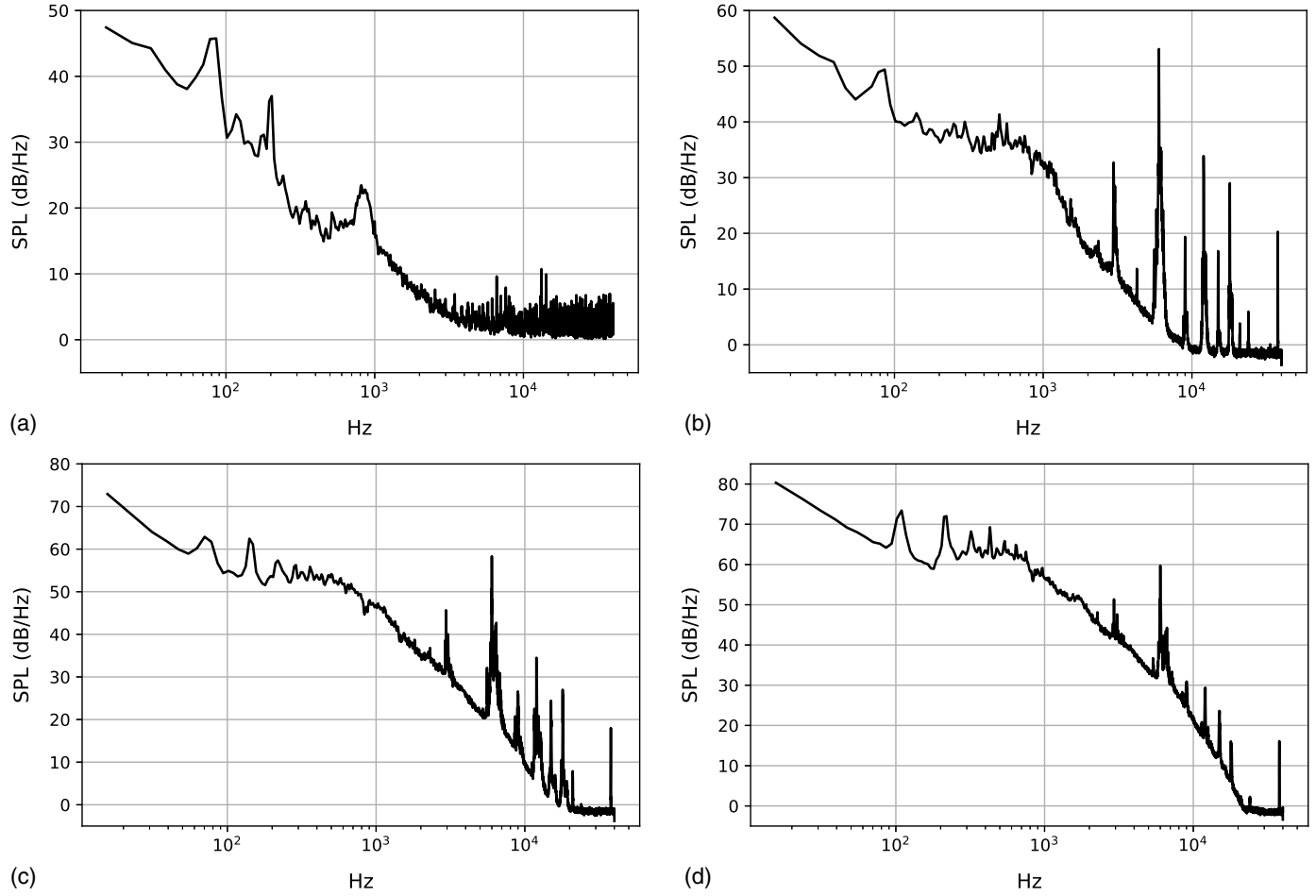

Fig. 9. Wind tunnel background noise spectra at different revolutions per minute with $EH = 0$: (a) U_{ref} = 0 m/s; (b) U_{ref} = 3.474 m/s; (c) U_{ref} = 6.853 m/s; and (d) U_{ref} = 10.619 m/s.

Table 1. UFBLWT working conditions for Stage 2 tests

Stage 2 UFBLWT background noise characterization (recordings with sampling frequency at 80 kHz)						
Test number	Speed estimated, WS (m/s)	Reference wind speed, U_{ref} (m/s)	Ambient temperature (°C)	Ambient pressure (Pa)	Humidity (%)	Fan speed (rpm)
1	0	0	29.7	1,016.6	45.6	0
2	2	1.705	29.9	1,016.4	44.1	120
6	4	3.357	29.5	1,016.1	41.6	240
7	6	4.825	29.6	1,016.2	41.6	360
8	8	6.793	29.8	1,016	42.1	480
9	10	8.56	29.8	1,016	41.5	600
10	12	10.47	30.2	1,016	40.5	720
11	15	13.351	29.7	1,015.7	42.2	900
12	12	10.47	30.2	1,016	40.5	720
13	10	8.457	29.9	1,015.9	41.4	600
14	8	6.619	29.8	1,016.1	41.8	480
15	6	4.836	29.6	1,016.2	41.6	360
16	4	3.356	29.6	1,016.1	40.2	240
17	2	1.705	29.9	1,016.4	44.1	120

tunnel frequencies. The characteristic peak frequencies were generated by the electric motors and the fan blades. The frequencies of the acoustic waves were set at 800, 1,250, 1,600, and 2,000 Hz to avoid these high-amplitude background noises. Table 1 presents the working conditions of this stage, including test numbers, estimated wind speed WS, measured reference wind speed U_{ref}, temperature, ambient pressure, and humidity.

Stage 3: UFBLWT Acoustic Propagation Experiment

The acoustic system consisted of the speaker system and the microphone system (Fig. 2). During this stage, the TCP was removed from the wind tunnel. There was no refraction of acoustic waves because the temperature variation was negligible in the tunnel. The *EL* values of the speaker and microphone varied within the test matrix, but always were equal to each other in any given

Downloaded from ascelibrary.org by Tianshu Zhang on 02/17/22. Copyright ASCE. For personal use only; all rights reserved.

Table 2. Parameters of Stage 3 with corresponding values

Stage 3 UFBLWT acoustic propagation experiment (recordings with sampling frequency at 40 kHz)	
Parameter	Values
Elevation height of acoustic system, EL (mm)	170, 590, 740, 900
Element height of ground element, EH (mm)	0, 10, 30, 50
Estimated wind speed, WS (m/s)	2, 4, 5, 6, 7, 8, 9, 10
Frequency of the acoustic wave, Frq (Hz)	1,250, 1,600, 2,000

experiment. This resulted in a horizontal straight-line ray path of the acoustic wave between the speaker face and microphone. The microphone was a G.R.A.S. 46BE ¼-in. (Holte, Denmark) CCP free-field microphone, which consisted of an IEC 61094 WS3F standardized G.R.A.S. 40BE ¼-in. prepolarized free-field microphone and a G.R.A.S. 26CB ¼-in. CCP standard preamplifier. The microphone frequency range was 4–80 kHz, and the dynamic range was 35–160 dB.

The microphone was placed at the center of the test section and pointed in the x-direction with 0° incident angle. When the wind tunnel flow passed the microphone, the turbulence generated by the microphone produced unwanted pressure variations on the microphone's diaphragm (Allen and Soderman 1993). Therefore, a G.R.A.S. RA0022 ¼-in. nosecone was placed on the microphone face to reduce the microphone self-noise. Fig. 4 shows how the microphone set was mounted on the height-adjustable supporting system with a range of 0–1,200 mm in the z-direction. A BNC cable connected the microphone to an amplifier, which transmitted the voltage signal to a data-acquisition (DAQ) system. The sampling frequency of the DAQ system was 40 kHz, and the DAQ system was controlled by LabView software version 2019. The microphone was calibrated before and after each acoustic test with a G.R.A.S. 42AG multifunction sound calibrator. The DAQ recorded both the voltage in volts and the acoustic pressure in pascals based on the acoustic calibration.

Fig. 5 shows the speaker system, which allowed the diaphragm to be moved vertically in the same range and increments as the microphone system. The speaker was controlled by a computer that was located outside the tunnel, near the fanbank. A MATLAB code was used to generate and play the test signal. A repeatable output was obtained from the speaker as in Stage 1.

The acoustic tests were performed based on an acoustic test matrixof 144 different tests (Table 2). Each test was defined by four different parameters: EL, terraformer element height EH, WS, and the frequency of the acoustic wave Frq. The EL heights were 170, 590, 740, and 900 mm in the z-direction. The terraformer configurations were homogeneous (all the elements maintained at the same height) for any test, with EH values were 0, 10, 30, and 50 mm. At the exit of the tunnel, a meteorological station was used to monitor the ambient pressure, humidity, and temperature (Fernández-Cabán and Masters 2020), which were recorded in the acoustic test matrix.

There was a total of nine WS values: 0, 2, 4, 5, 6, 7, 8, 9, and 10 m/s. The Frq values considered in this series of tests were 1,250, 1,600, and 2,000 Hz.

Stage 4: UFBLWT Turbulent Measurements

To obtain the turbulent statistics along the ray path, the TCP was placed at the same z location as the acoustic system's EL, and the acoustic system was removed in this stage. Turbulent flow-fields were measured using Cobra probes mounted on an automated multiple-degree-of-freedom instrument gantry which was capable of traversing longitudinally, laterally, and vertically nearly the entire length, width, and height of the test section (Catarelli et al. 2020b).

Fig. 10. Coordinates calibration of TCP system at $z_b = 590$ mm.

Table 3. Parameters of Stage 4 with corresponding values

Stage 4 UFBLWT turbulent measurements (measurements with sampling frequency at 2 kHz)		
	Values	
Parameter	Config A	Config B
x-location of TCP system, X (m)	2, 20	10, 16
z-location of bottom probe in TCP, Z_b (mm)	170, 590, 740, 900	170, 490, 640, 800
Element height of ground element, EH (mm)	0, 30	0, 30
Estimated wind speed, WS (m/s)	6, 8, 10	6, 8, 10

The TCP system consisted of three identical Cobra probes (Turbulent Flow Instrumentation, Victoria, Australia). Each Cobra probe was a fast-response four-hole probe capable of measuring three-dimensional fluctuating velocity components with a sampling frequency of 2 kHz. We defined the as-measured velocity component in the x-direction as U_{probe}. For any one gantry position, the TCP system collected the data simultaneously at three vertical locations.

Fig. 10 shows the assembled TCP system. Cobra probes were labeled with the numbers 272, 266, and 256 (from low to high elevation). The height of the bottom Cobra probe, 272, z_b, represented the vertical location of the TCP system. The spacing between Probes 272 and 266 (middle probe) was 40 mm, and the spacing between Probes 266 and 256 (top probe) was 60 mm. By this arrangement, a vertical profile of turbulence was obtained with 12 measuring points with 4 TCP z_b locations. Those profiles can be tracked in the DesignSafe data by directly searching for the z-location of the measuring point.

The Stage 4 test matrix included a total of 96 different tests (Table 3). Each test was defined by four different parameters: z_b, EH, the TCP position in the x-direction (X), and WS. To measure the turbulence along the ray path, two TCP vertical arrangements were employed. The first arrangement was for $x = 2$ and 20 m. The z-location of Probe 272, z_b, was set to be identical to the value of EL (170, 590, 740, and 900 mm) in the acoustic test. For the cases with $x = 10$ and 16 m, the z_b in the second arrangement was set at 170, 490, 640, and 800 mm. In the second arrangement, the turbulence along the ray path was measured by Probe 256 for $EL = 590$, 740, and 900 mm, because Probe 256 was 100 mm

Downloaded from ascelibrary.org by Tianshu Zhang on 02/17/22. Copyright ASCE. For personal use only; all rights reserved.

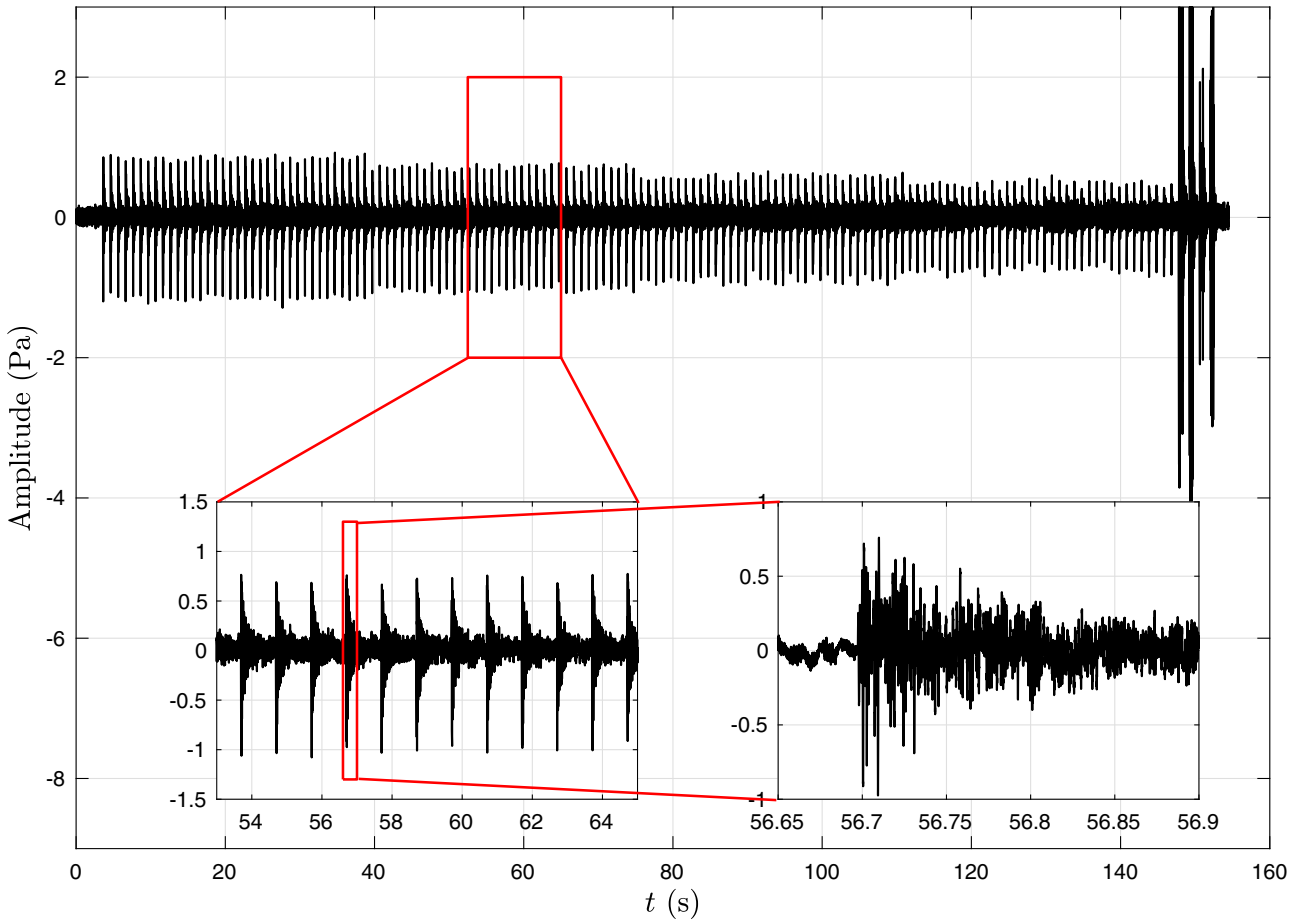

Fig. 11. Wind tunnel recording with $EH = 30$ mm, $EL = 590$ mm, and WS $= 4$ m/s.

higher than Probe 272. The EHs were set to be 0 and 30 mm to generate two types of boundary layer profiles with roughness length (z_0) values of 0.00017 and 0.025 m, respectively, according to Catarelli et al. (2020a). In this set of tests, the three wind speeds WS were 6, 8, and 10 m/s. Stage 1 and Stage 2 were considered to be experimental preparation, whereas Stage 3 and Stage 4 were experimental results.

Sample Experimental Results

This section presents and discusses sample results for Stage 3 and Stage 4 tests. All the parameters in this section are introduced in Tables 2 and 3. In this section, the acoustic waves recorded in UFBLWT are presented as both raw recordings and postprocessed signals. Sample results of the turbulent measurements, including energy spectra of turbulent velocity, mean u-component profiles, turbulent kinetic energy (TKE), and turbulent intensity, are presented. The detailed data structure and data depot organization are described in the following sections.

Acoustic Recordings and Signal Postprocessing

Fig. 11 shows a recording from Stage 3 in the wind tunnel at $WS = 4$ m/s and roughness element height $EH = 30$ mm without any postprocessing.

The entire acoustic signal consisted of five parts as designed and discussed previously (Fig. 6). The bottom-left inset in Fig. 11 presents a part of the 1,250 Hz signal, clearly showing the periodic signal as 12 pulses. The bottom-right inset is an example of a recorded pulse, in which the first crest occurs at $t = 56.7$s at 0.24 Pa. Reflected waves are shown after the single-cycle pulse, which are not present in Fig. 8. We choose to present this low wind speed case because the first crest is apparent, even with trailing reflected waves. However, for higher wind speeds, the background noise increases significantly while the acoustic signal volume remains constant. As wind speed increases, the signal-to-noise ratio can be less than 1, which make the first crest hard to recognize.

To separate background noise from the acoustic signal, we ensemble-averaged 36 1-s segments associated with each of the 1,250, 1,600, and 2,000 Hz signals. Fig. 12 shows one example of an ensemble-averaged signal at 1,250 Hz.

Applying the ensemble average significantly reduced the background noise. For example, in a case with increased mean wind speed and turbulence (WS m/s, $EH = 30$ mm, $EL = 590$ mm, and $Frq = 1{,}250$ Hz), the signal-to-noise ratio increased from 0.229 to 2.817 via ensemble averaging. In Fig. 12 the first sine wave is clearly recognizable, along with the trough's impulse response, causing about a 50% increment in magnitude, which is same as the result obtained from the anechoic chamber test (Fig. 8). After 2 ms, the signal completely lost its original waveform, which possibly was caused by the interference of reflected waves. The signal's amplitude decreased with increasing U_{ref} from 0 to 7.8 m/s. The turbulent scattering effect on the acoustic wave propagation is considered to be a type of attenuation similar to atmospheric absorption. Comparing the test signals with $U_{\text{ref}} = 7.8$ m/s and zero wind speed shows an additional SPL decrease of 0.1214 dB/m, whereas the atmospheric attenuation was

Downloaded from ascelibrary.org by Tianshu Zhang on 02/17/22. Copyright ASCE. For personal use only; all rights reserved.

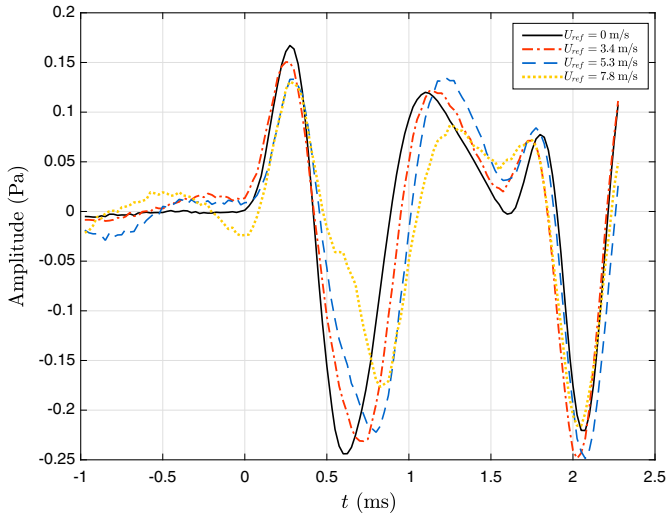

Fig. 12. Ensemble signal of 1,250 Hz with $EH = 30$ mm and $EL = 590$ mm.

0.0608 dB/m for this case at 24.3°C, 100.86 kPa pressure, and 49.2 % humidity (Sutherland and Bass 2004). The authors currently are investigating a potential empirical model to account for this attenuation.

Turbulent Statistics of Tests: Stage 4

The instantaneous velocity with three orthogonal components was measured by the TCP system (Foken and Nappo 2008). Fig. 13 presents the power spectral density (PSD) of the fluctuating component of wind in the x-direction, defined as the turbulent velocity u' for a test at $z_b = 170$ mm, WS = 10 m/s, $x = 2$ m, and $EH = 0$ and 30 mm; $E(k)$ is the energy-spectrum function, where k is the wavenumber of the u-component turbulent velocity. As expected, $k^{-5/3}$ energy decay was observed in the inertial range.

Fig. 14 illustrates the boundary layer mean velocity profiles at $x = 20$, 16, 10, and 2 m with the coordinate system provided in Fig. 2. The x-axis U_{probe} represents the wind velocity measured by each single Cobra probe. The longitudinal turbulent intensity profiles are shown in Fig. 15.

The x-axis represents the longitudinal turbulent intensity I_u. The turbulent intensity decreased with increasing z for all four x-locations. The vertical-spatial-averaged turbulent intensity decreased from 12.42% at $x = 20$ m to 7.42% at $x = 2$ m.

The purpose of the precediung discussion of turbulence profiles along the center line of the UFBLWT is to inform the modeling of the effect of turbulence on acoustic propagation from speaker to microphone. One possible approach to analyze the acoustic–turbulent interaction is the Lighthill's scattering coefficient (Lighthill 1956)

$$\alpha = \frac{8\pi L_1}{\Lambda^2} I \frac{\overline{u'^2}}{c^2} \tag{4}$$

where L_1 = integral length scale; Λ = wavelength of acoustic wave; I = intensity of acoustic wave; and c = wave speed of acoustic wave. In Eq. (4), the term $\overline{u'^2}$ is a significant parameter to analyze the turbulent effect on acoustic propagation, which is related to the turbulent kinetic energy. Here, TKE is defined as $(1/2)\langle u_i u_i \rangle$ (Pope 2001), and the TKE measurements are presented in the following paragraph. Knowledge of the integral length scale is critical for making accurate long-range predictions; however, there are multiple ways to estimate it. The methodology to estimate the integral length scale varies (Iyengar and Farell 2001), and results in different values from one-point data. Therefore, the length scale results are not presented here; readers may use their preferred method for its calculation.

Fig. 16 presents the TKE measurements along the ray path for different x-locations. The x-axis represents the U_{probe}, and the y-axis is the TKE. At each x-location, the TKE decreased with increasing z, which agrees with previous measurements. From the upstream location of $x = 20$ m to the location nearest to the test section at $x = 2$ m, the TKE decreased dramatically because of the dissipation effect on the wind tunnel flow. The maximum TKE at the near the inlet location ($x = 20$ m) was 0.7756 m^2/s^2, whereas the TKE at the location closest to the test section ($x = 2$ m) was 0.1507 m^2/s^2.

Data Organization

Fig. 17 shows the structure of the data in the DesignSafe-CI Data Depot repository. The documentation includes a data dictionary, the

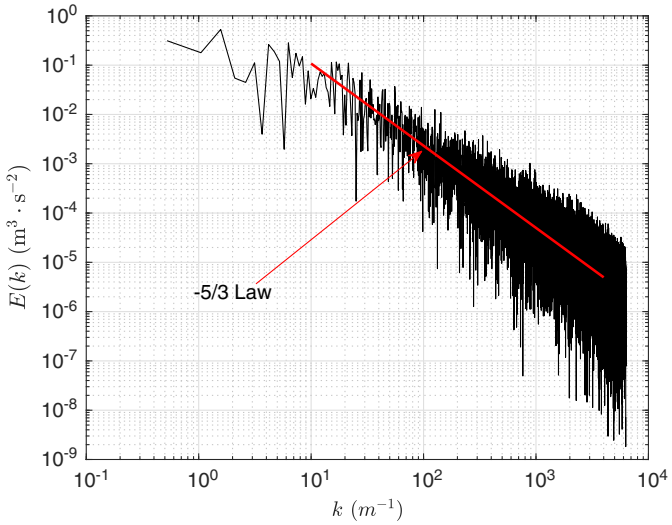

Fig. 13. PSD of u' at $EH = 30$ mm, $z_b = 170$ mm, WS = 10 m/s, and $x = 2$ m.

Downloaded from ascelibrary.org by Tianshu Zhang on 02/17/22. Copyright ASCE. For personal use only; all rights reserved.

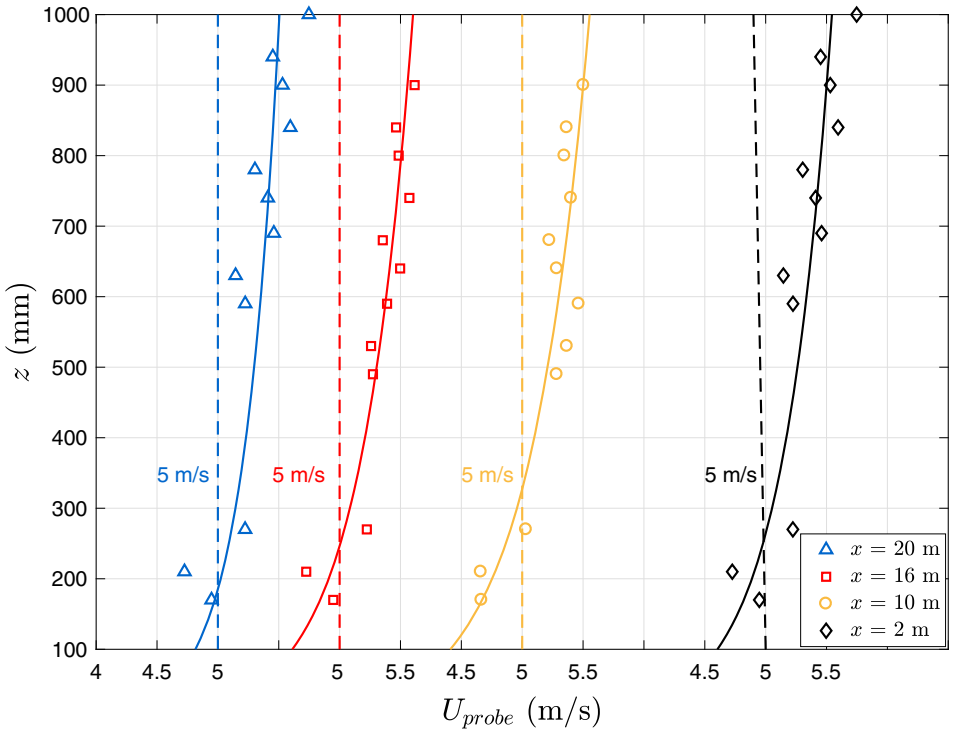

Fig. 14. Boundary layer profiles along the x-direction, with $EH = 30$ mm and WS $= 6$ m/s.

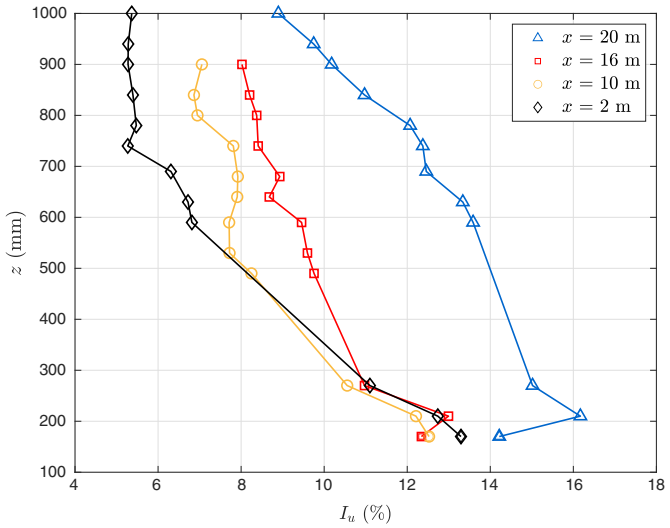

Fig. 15. Longitudinal turbulent intensity I_u with $EH = 30$ mm and WS $= 6$ m/s.

test matrixes, the specifications of the instrumentation used for the experiments, and the data set obtained in each stage of the experimental procedure. The data set consists of four major events: (1) the anechoic test, (2) the UFBLWT background noise characterization, (3) the UFBLWT acoustic propagation experiment, and (4) the UFBLWT turbulent measurements. The data files for each event are described subsequently. The anechoic test section includes the recorded acoustic signals in the anechoic chamber at 2 and 3 m from the speaker, which are stored as SourceSignal_2 m.mat and SourceSignal_3 m.mat files, respectively. The recorded signal is the pressure signal (pascals) with a sampling frequency 40 kHz.

The background noise characterization section contains a total of 14 background recordings. The file UFBLWTCharacterizationMatrix.xlsx in the Stage 2 folder was used to track each test with its test numbers and with the operating conditions such as measured wind speed (meters per ssecond), temperature (degrees Celsius), ambient pressure (pascals), and humidity (percent). Each test from Background_test_1 to Background_test_14 is organized as a MATLAB matrix with two columns. The first column is the recording of the voltage signal (volts), and the second column is the pressure signal (pascals); the sampling frequency of these recordings was 80 kHz.

the acoustic propagation data folder section is into acoustic raw data subfolders (part 1 and part 2) and the Acoustic.mat file. The raw acoustic data subfolder includes each of the 144 acoustic recordings without postprocessing. The first 100 tests are located in Acoustic Raw Data Folder Part 1, and the 44 remaining tests are located in Acoustic Raw Data Folder Part 2. Each file is organized as a MATLAB matrix with two columns, the same as the background characterization recordings. The sampling frequency of these files was 40 kHz. The Acoustic.mat file includes the postprocessed acoustic data. The file is in a cascade structure, and a time series are loaded after each of the four fields is selected: EL, EH, WS, and Frq. For example, if the user requires a recording of a specific acoustic test with $EL = 590$ mm, $EH = 30$ mm, WS $=$ 5 m/s, and $Frq = 1{,}250$ Hz, it is possible to access the pressure–time history recording through the next prompt after the MATLAB file Acoustic·EL590·EH30.Wind5.Frq1250 has been loaded. In the Acoustic_Test_Matrix.xlsx file, the user can track the characteristics of the data they want to visualize.

The turbulent measurements data folder section is organized into two types of files: Realtime_Turbulence.mat and Turbulence.mat files. The Realtime_Turbulence.mat file includes the instantaneous flow velocity measurements (meters per second), structured in five different fields: the component (Comp_u, Comp_v, or Comp_w), EH, WS, X, and Z. In the turbulent data

Downloaded from ascelibrary.org by Tianshu Zhang on 02/17/22. Copyright ASCE. For personal use only; all rights reserved.

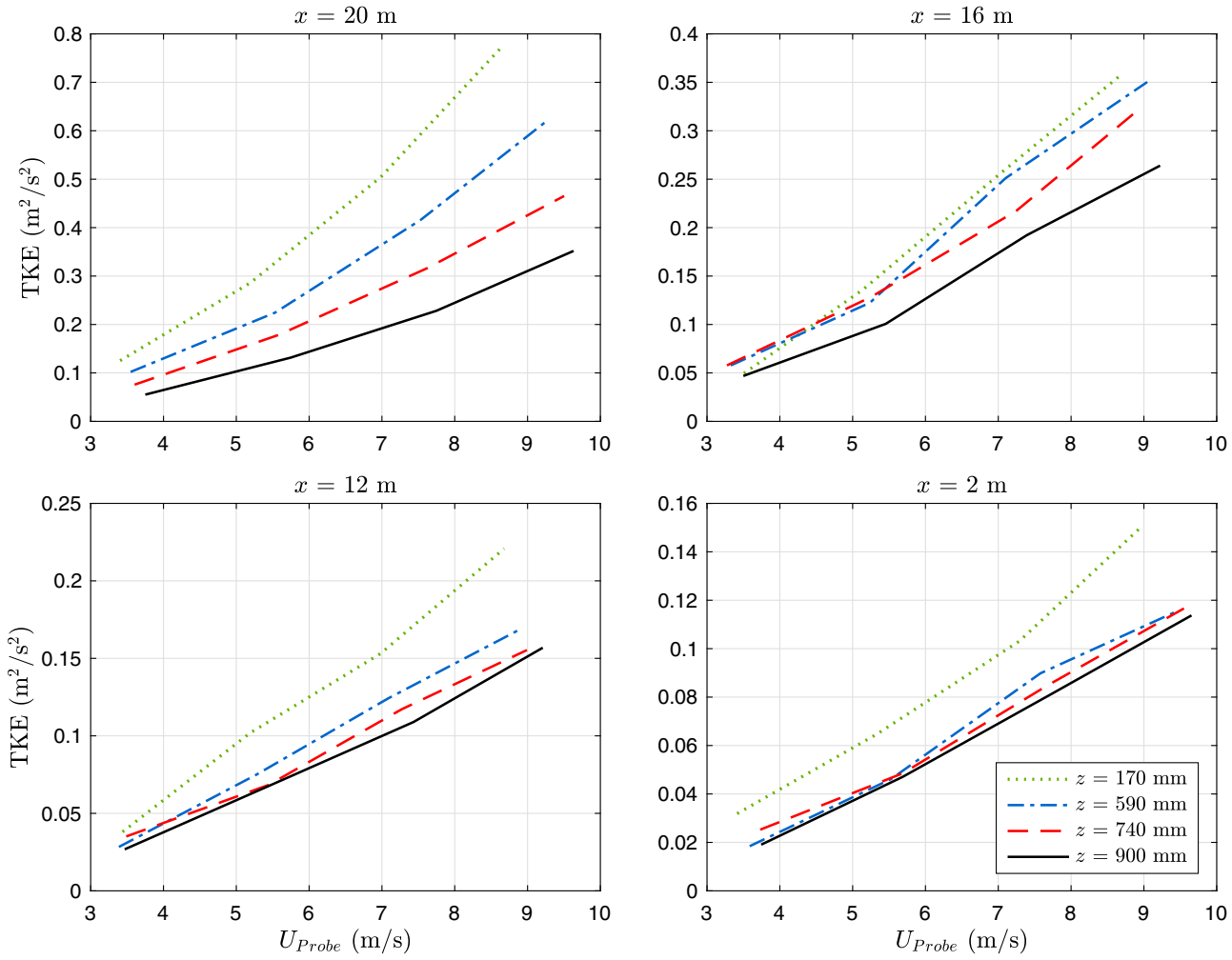

Fig. 16. TKE measurements with $EH = 0$.

sets, the parameter X represents the location on the x-axis, and Z represents the elevation of the Cobra probe on the z-axis. The file is in a cascade structure, and a time series is loaded after each of the five fields is selected. The first field corresponds to the component, i.e., comp_u, comp_v, or comp_w (along wind, across wind, and vertical components). For example, if the user wants to know the instantaneous flow velocity specifically for the component u, $EH = 30$ mm, WS $= 10$ m/s, $x = 2$ m, and $z = 590$ mm, it is possible to access the time history through the next prompt after the MATLAB file Realtime_Turbulence. Comp_u·EH30·WS10·X2·Z590 has been loaded. The Turbulence.mat file includes the postprocessed turbulent measurements, and it has a cascade structure. In this case, there are three different fields: X, Z, and EH. After each field has been selected, it is possible to access the different parameters for the group of turbulent statistics, such as the mean velocity (MeanVelocityU), the TKE, and the turbulent intensity (TI). For example, if the user requires data from the Turbulence.mat file with $x = 20$ m, $z = 590$ mm, and $EH = 30$ mm, it is possible access to the information through the next prompt after the MATLAB file Turbulence·X20·Z590·EH30 has been loaded. After the file is loaded, for each turbulent parameter field, three values of this parameter are loaded as an array. The indexes of the elements in the array, 1, 2, and 3, corresponds to the WS at 6, 8, and 10 m/s.

Discussion

The major purpose of this study was to offer a publicly accessible data set of acoustic wave propagation in a turbulent medium. Based on the experiments, the acoustic–turbulence interaction was observed as an attenuation effect, because the amplitude of the acoustic signal decreased with increasing turbulence intensity. One major application of the data set is tornadic or other supercell storm infrasound propagation through the atmosphere (Bowman and Bedard 1971; Noble and Bedard 2006). A numerical solver to predict the tornado formation with the generalized Burgers' equation uses this data set to account for the turbulence effects (Zhang and Miller 2020).

Infrasound generated in and propagated through the atmosphere by other events such as explosions, earthquakes, and volcanic eruptions also can be investigated with this data set for their far-field propagation (Bedard and Georges 2000). The implementations of acoustic propagation approaches, such as the generalized Burgers' equation (Blackstock 1969) and the parabolic equation (Blanc-Benon et al. 2002), can be validated by use of this data set.

Currently, there is no wind tunnel that can create perfectly scaled atmospheres relative to the full atmospheric turbulent boundary layer (Cook 1978; Van Pelt et al. 2010; Cook 2021). The turbulent boundary layer created within the UFBLWT does

Downloaded from ascelibrary.org by Tianshu Zhang on 02/17/22. Copyright ASCE. For personal use only; all rights reserved.

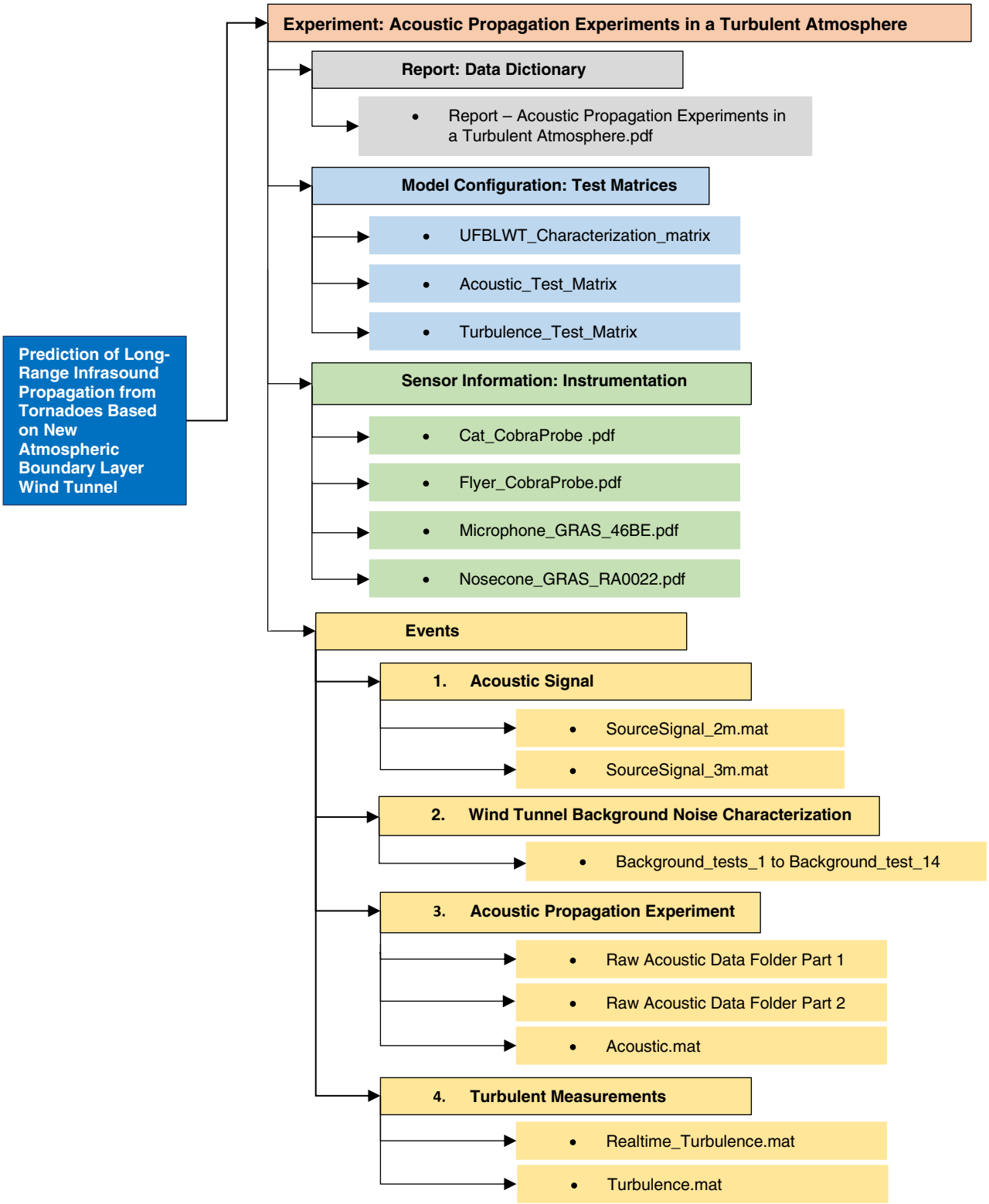

Fig. 17. Data depot structure.

not capture atmospheric temperature and density fluctuations. Therefore, we do not expect the acoustic data from the UFBLWT to include the effects of acoustic refraction (Brown and Hall 1978) due to the mean density gradients that are present in the atmosphere. However, the tunnel does allow acoustic waves to be modified by turbulence, as observed in the present measurements. Furthermore, the wind tunnel is not an anechoic facility. The acoustics contain reflections from the walls of the tunnel. Waves in the facility follow a system described by Vaidya and Dean (1977), which correspond to duct acoustics (Pridmore-Brown 1958). To overcome this tunnel limitation, an ensemble-averaging technique to capture the direct ray and its effects from turbulence

J. Struct. Eng., 2022, 148(5): 04722001

Downloaded from ascelibrary.org by Tianshu Zhang on 02/17/22. Copyright ASCE. For personal use only; all rights reserved.

was implemented. This method allowed us to remove the reflected waves from the tunnel walls, floor, and ceiling. Such reflections can be eliminated in practice from three of the walls of a wind tunnel by performing similar acoustic experiments in a wall-jet facility (Chong et al. 2009), but no such wall-jet wind tunnel with roughness elements exists. Finally, only a limited number of measurements along the ray paths of the acoustic waves from source to observer were captured by the TCP system. This limitation is not a major issue because of the nature of the slowly varying boundary layer (Schlichting and Gersten 2016) after its initial rapid development near the tunnel entrance. In practice, these profiles are interpolated between measurement positions to approximate the entire profile for the validation of acoustic prediction codes.

Data Availability Statement

Some or all data, models, or code that support the findings of this study are available from the corresponding author upon reasonable request. Some or all data, models, or code generated or used during the study are available in a repository online in accordance with funder data retention policies. The online data are published on DesignSafe and are accessible via https://doi.org/10.17603/ds2-bpav-8w29.

Acknowledgments

The authors are grateful for continual funding from NOAA. This program is supported by the NOAA Weather and Air Quality Research program Award No. NA18OAR4590306. The authors are grateful for the technicians and staff at the National Science Foundation Boundary Layer Wind Tunnel at the University of Florida.

Notation

The following symbols are used in this paper:

c = speed of sound;
EH = pitch height of ground element;
$E(k)$ = turbulent energy spectrum;
EL = elevation height of acoustic system;
Frq = frequency of test signal;
f = frequency;
H = Heaviside function;
I = intensity of acoustic wave;
I_u = longitudinal turbulent intensity;
k = turbulent wavenumber;
L_1 = integral length scale;
N = number of sampling points;
S_s = sine wave function;
S_t = test signal;
t = time;
U_{probe} = velocity at Cobra probe;
U_{ref} = velocity of tunnel measured by pitot probe;
u' = turbulent velocity;
W_t = window function;
WS = estimated wind speed;
X = three-Cobra-probe axial location;
Z = elevation of three-Cobra-probe system;
z_b = vertical location of three-Cobra-probe system;
z_0 = roughness length;
α = turbulent attenuation coefficient; and
λ = wavelength of acoustic wave.

References

Allen, C., and P. Soderman. 1993. "Aeroacoustic probe design for microphone to reduce flow-induced self-noise." In *Proc., 15th Aeroacoustics Conf.* Reston, VA: American Institute of Aeronautics and Astronautics.

Aoshima, N. 1981. "Computer-generated pulse signal applied for sound measurement." *J. Acoust. Soc. Am.* 69 (5): 1484–1488. https://doi.org/10.1121/1.385782.

Baals, D. D. 1981. Vol. 440 of *Wind tunnels of NASA*. Washington, DC: Scientific and Technical Information Branch, National Aeronautics and Space Administration.

Bedard, A. J. 2005. "Low-frequency atmospheric acoustic energy associated with vortices produced by thunderstorms." *Mon. Weather Rev.* 133 (1): 241–263. https://doi.org/10.1175/MWR-2851.1.

Bedard, A. J., Jr., B. W. Bartram, A. N. Keane, D. C. Welsh, and R. T. Nishiyama. 2004. "The infrasound network (ISNet): Background, design details, and display capability as an 88d adjunct tornado detection tool." In *Proc., 22nd Conf. on Severe Local Storms*. Bostan: American Meteorological Society.

Bedard, A. J., Jr., and T. M. Georges. 2000. "Atmospheric infrasound." *Phys. Today* 53 (3): 32–37. https://doi.org/10.1063/1.883019.

Blackstock, D. 1969. "History of nonlinear acoustics and a survey of burgers' and related equations." In *Proc., Nonlinear Acoustics, Symp. held at Applied Research Laboratories*, 1–27. Austin, TX: Univ. of Texas Austin.

Blanc-Benon, P., B. Lipkens, L. Dallois, M. F. Hamilton, and D. T. Blackstock. 2002. "Propagation of finite amplitude sound through turbulence: Modeling with geometrical acoustics and the parabolic approximation." *J. Acoust. Soc. Am.* 111 (1): 487–498. https://doi.org/10.1121/1.1404378.

Bowman, H. S., and A. J. Bedard. 1971. "Observations of infrasound and subsonic disturbances related to severe weather." *Geophys. J. R. Astron. Soc.* 26 (1–4): 215–242. https://doi.org/10.1111/j.1365-246X.1971.tb03396.x.

Brooks, H. E., and C. A. Doswell III. 2001. "Normalized damage from major tornadoes in the United States: 1890–1999." *Weather Forecasting* 16 (1): 168–176. https://doi.org/10.1175/1520-0434(2001)016<0168:NDFMTI>2.0.CO;2.

Brouwer, H. H. 1997. *Anechoic wind tunnels*. Bangalore, India: National Aerospace Laboratory.

Brown, E. H., and F. F. Hall Jr. 1978. "Advances in atmospheric acoustics." *Rev. Geophys.* 16 (1): 47. https://doi.org/10.1029/RG016i001p00047.

Catarelli, R. A., P. L. Fernández-Cabán, F. J. Masters, J. A. Bridge, K. R. Gurley, and C. J. Matyas. 2020a. "Automated terrain generation for precise atmospheric boundary layer simulation in the wind tunnel." *J. Wind Eng. Ind. Aerodyn.* 207 (Dec): 104276. https://doi.org/10.1016/j.jweia.2020.104276.

Catarelli, R. A., P. L. Fernández-Cabán, B. M. Phillips, J. A. Bridge, F. J. Masters, K. R. Gurley, and D. O. Prevatt. 2020b. "Automation and new capabilities in the university of Florida NHERI Boundary Layer Wind Tunnel." *Front. Built Environ.* 6: 558151. https://doi.org/10.3389/fbuil.2020.558151.

Chong, T. P., P. F. Joseph, and P. O. A. L. Davies. 2009. "Design and performance of an open jet wind tunnel for aero-acoustic measurement." *Appl. Acoust.* 70 (4): 605–614. https://doi.org/10.1016/j.apacoust.2008.06.011.

Cook, N. J. 1978. "Wind-tunnel simulation of the adiabatic atmospheric boundary layer by roughness, barrier and mixing-device methods." *J. Wind Eng. Ind. Aerodyn.* 3 (2–3): 157–176. https://doi.org/10.1016/0167-6105(78)90007-7.

Cook, N. J. 2021. "Comment to 'Atmospheric boundary layer modeling in a short wind tunnel' by Dan Hlevca and Mircea Deguratu, EJM/B Fluids, 79 (2020), 367-375." *Eur. J. Mech. B Fluids* 85 (Jan): 397–399. https://doi.org/10.1016/j.euromechflu.2020.08.007.

Duell, E. G., J. Walter, J. Yen, and T. Nagle. 2013. "Progress in aeroacoustic and climatic wind tunnels for automotive wind noise and acoustic

Downloaded from ascelibrary.org by Tianshu Zhang on 02/17/22. Copyright ASCE. For personal use only; all rights reserved.

testing." *SAE Int. J. Passenger Cars Mech. Syst.* 6 (1): 448–461. https://doi.org/10.4271/2013-01-1352.
Elbing, B. R., C. E. Petrin, and M. S. Van Den Broeke. 2018. "Detection and characterization of infrasound from a tornado." In *Proc., 175th Meeting of the Acoustical Society of America*, 1–40. Melville, NY: Acoustical Society of America.
Everest, F. A. 2001. *Master handbook of acoustics*. New York: McGraw-Hill.
Evers, L. G., and H. W. Haak. 2010. "The characteristics of infrasound, its propagation and some early history." In *Infrasound monitoring for atmospheric studies*, 3–27. Dordrecht, Netherlands: Springer.
Fernández-Cabán, P., F. Masters, and B. Phillips. 2018. "Predicting roof pressures on a low-rise structure from freestream turbulence using artificial neural networks." *Front. Built Environ.* 4 (Nov): 68. https://doi.org/10.3389/fbuil.2018.00068.
Fernández-Cabán, P. L., and F. J. Masters. 2018. "Effects of freestream turbulence on the pressure acting on a low-rise building roof in the separated flow region." *Front. Built Environ.* 4 (Apr): 17. https://doi.org/10.3389/fbuil.2018.00017.
Fernández-Cabán, P. L., and F. J. Masters. 2020. "Experiments in a large boundary layer wind tunnel: Upstream terrain effects on surface pressures acting on a low-rise structure." *J. Struct. Eng.* 146 (8): 04720002. https://doi.org/10.1061/(ASCE)ST.1943-541X.0002690.
Foken, T., and C. Nappo. 2008. *Micrometeorology*. Berlin: Springer.
Frazier, W. G., C. Talmadge, J. Park, R. Waxler, and J. Assink. 2014. "Acoustic detection, tracking, and characterization of three tornadoes." *J. Acoust. Soc. Am.* 135 (4): 1742–1751. https://doi.org/10.1121/1.4867365.
Holloway, C. L., P. M. McKenna, R. A. Dalke, R. A. Perala, and C. L. Devor. 2002. "Time-domain modeling, characterization, and measurements of anechoic and semi-anechoic electromagnetic test chambers." *IEEE Trans. Electromagn. Compat.* 44 (1): 102–118. https://doi.org/10.1109/15.990716.
Iyengar, A. K. S., and C. Farell. 2001. "Experimental issues in atmospheric boundary layer simulations: Roughness length and integral length scale determination." *J. Wind Eng. Ind. Aerodyn.* 89 (11–12): 1059–1080. https://doi.org/10.1016/S0167-6105(01)00099-X.
Le Pichon, A., E. Blanc, and A. Hauchecorne. 2010. *Infrasound monitoring for atmospheric studies*. Dordrecht, Netherlands: Springer.
Lighthill, M. J. 1956. "Viscosity effects in sound waves of finite amplitude." In *Surveys in mechanics*. Cambridge, UK: Cambridge University Press.
Mäkivirta, A., J. Liski, and V. Välimäki. 2018. "Modeling and delay-equalizing loudspeaker responses." *J. Audio Eng. Soc.* 66 (11): 922–934. https://doi.org/10.17743/jaes.2018.0053.
Mathew, J., C. Bahr, B. Carroll, M. Sheplak, and L. Cattafesta. 2005a. "Design, fabrication, and characterization of an anechoic wind tunnel facility." In *Proc., 11th AIAA/CEAS Aeroacoustics Conf.* Reston, VA: American Institute of Aeronautics and Astronautics.
Mathew, J., C. Bahr, M. Sheplak, B. Carroll, and L. N. Cattafesta. 2005b. "Characterization of an anechoic wind tunnel facility." In *Proc., Noise Control and Acoustics*. New York: ASME.
Noble, J. M., and A. J. Bedard Jr. 2006. "Infrasound from tornadoes and other severe storms." *J. Acoust. Soc. Am.* 120 (5): 3031. https://doi.org/10.1121/1.4787148.
Pepyne, D., M. Zink, J. Brotzge, E. Knapp, A. Mendes, B. McCarthy, S. Klaiber, and B. Benito-Figueroa. 2011. "An integrated radar-infrasound network for meteorological infrasound detection and analysis." In *Proc., 91st American Meteorological Society Annual Meeting*. Boston: American Meteorological Society.
Pope, S. B. 2001. *Turbulent flows*. Cambridge, UK: Cambridge University Press.
Pridmore-Brown, D. C. 1958. "Sound propagation in a fluid flowing through an attenuating duct." *J. Acoust. Soc. Am.* 30 (7): 670. https://doi.org/10.1017/S0022112058000537.
Remillieux, M., E. Crede, H. Camargo, R. A. Burdisso, W. Devenport, M. Rasnick, P. Van Seeters, and A. Chou. 2008. "Calibration and demonstration of the new Virginia Tech anechoic wind tunnel." In *Proc., 14th AIAA/CEAS Aeroacoustics Conf. (29th AIAA Aeroacoustics Conf.)*. Reston, VA: American Institute of Aeronautics and Astronautics.
Schimmel, A., and J. Hübl. 2015. "Approach for an early warning system for debris flow based on acoustic signals." In Vol. 3 of *Engineering geology for society and territory*, 55–58. Cham, Switzerland: Springer.
Schlichting, H., and K. Gersten. 2016. *Boundary-layer theory*. New York: Springer.
Sovardi, C., S. Jaensch, and W. Polifke. 2016. "Concurrent identification of aero-acoustic scattering and noise sources at a flow duct singularity in low Mach number flow." *J. Sound Vib.* 377 (Sep): 90–105. https://doi.org/10.1016/j.jsv.2016.05.025.
Sutherland, L. C., and H. E. Bass. 2004. "Atmospheric absorption in the atmosphere up to 160 km." *J. Acoust. Soc. Am.* 115 (3): 1012–1032. https://doi.org/10.1121/1.1631937.
Talmadge, C., and R. Waxler. 2016. "Infrasound from tornados: Theory measurement and prospects for their use in early warning systems." *Acoust. Today* 12 (1): 43–51.
Vaidya, P., and P. Dean. 1977. "The state of the art of duct acoustics." In *Proc., 4th Aeroacoustics Conf.* Reston, VA: American Institute of Aeronautics and Astronautics.
Van Pelt, R. S., T. M. Zobeck, M. C. Baddock, and J. J. Cox. 2010. "Design, construction, and calibration of a portable boundary layer wind tunnel for field use." *Trans. ASABE* 53 (5): 1413–1422. https://doi.org/10.13031/2013.34911.
Zhang, T., and S. A. Miller. 2020. "Toward prediction of tornado noise within the turbulent atmosphere using theory, wind tunnel measurements, and field-tests." In *Proc., AIAA Scitech 2020 Forum*. Reston, VA: American Institute of Aeronautics and Astronautics.

Downloaded from ascelibrary.org by Tianshu Zhang on 02/17/22. Copyright ASCE. For personal use only; all rights reserved.